13th International Symposium on Particle Image Velocimetry – ISPIV 2019
Munich, Germany, July 22-24, 2019

PIV-PTV comparison of the oscillating flow inside the human lungs

Thomas Janke[1*], Rüdiger Schwarze[1], Katrin Bauer[1]

[1] TU Bergakademie Freiberg, Institut für Mechanik und Fluiddynamik, Freiberg, Germany

[*] Thomas.Janke@imfd.tu-freiberg.de

Abstract

This work presents a comparative study between a Particle Tracking Velocimetry (PTV) and a Particle Image Velocimetry (PIV) image processing to obtain velocity fields within a realistic replica of the human airways. The oscillating flow within the refractive index matched model is set to a peak Reynolds number of $Re \approx 2000$ and a Womersley number of $\alpha = 1.9$. The aim of this study is the validation of the in-house developed PTV algorithm against a well-established PIV algorithm. The results indicate an overall good performance of the PTV implementation. In wall-near regions, the resolution of the velocity field can be improved by the PTV method at the cost of more noise. Different mean particle displacements are handled well by both evaluation approaches. Larger differences between PTV and PIV occur at the point of flow reversal with nearly zero mean velocity.

1 Introduction

A thorough knowledge about the flow within the human lung can help in improving existing ventilation strategies. In the past, a large amount of in vitro investigations on this topic, contributed by the fluid dynamics community, utilized the Particle Image Velocimetry (PIV) technique (e.g. Adler and Brücker (2007); Fresconi and Prasad (2007); Große et al. (2007)). While the technique reveals important parts of the flow, it goes along with certain drawbacks due to its image evaluation process. One of the most known limitations of PIV is the lacking ability of resolving wall-near flows because of its finite-sized interrogation windows Kähler et al. (2012). Another point arises, when investigating oscillatory flows as they occur within the human lungs. For these flows it is difficult to find a suitable image time separation, which matches the peak velocity phases as well as the flow reversal phases with near-zero velocities. A possibility to encounter the first limitation is the use of a Particle Tracking Velocimetry (PTV) image evaluation method. PTV offers the advantage of not only evaluating the flow velocities at relatively large interrogation windows but to obtain a velocity information for each detected seeding particle and, therefore, increasing the spatial resolution, when one is able to keep the seeding density comparable between PIV and PTV. This has been a problem in the past but with recent PTV algorithms, it is possible to reach similar seeding densities for PTV as they are used in PIV. One of these algorithms has been the method proposed by Fuchs et al. (2017), which reportedly works up to 0.06 particles per pixel. It is based on a statistical analysis of the motion of a local particle neighborhood and is also able to resolve strong velocity gradients. This means as well, that the algorithm is able to handle a broad range of possible particle displacements as they occur in an oscillating flow as in the human lungs. Based on these reported promising results, we implemented an in-house version of this algorithm to test its theoretical advantages. We further compare the results against a well-established, commercially available PIV algorithm with the aim of verifying the obtained PTV results.

2 Experimental set up

The investigated model of the human airways (see Fig. 1) is based on realistic patient-specific data and has been introduced by Koullapis et al. (2018) as a new benchmark geometry for the research on patient-specific drug delivery and has been firstly described by Lizal et al. (2012). The replicated model, based on the benchmark geometry, used in our study is made of a transparent silicone and has already been used for PIV

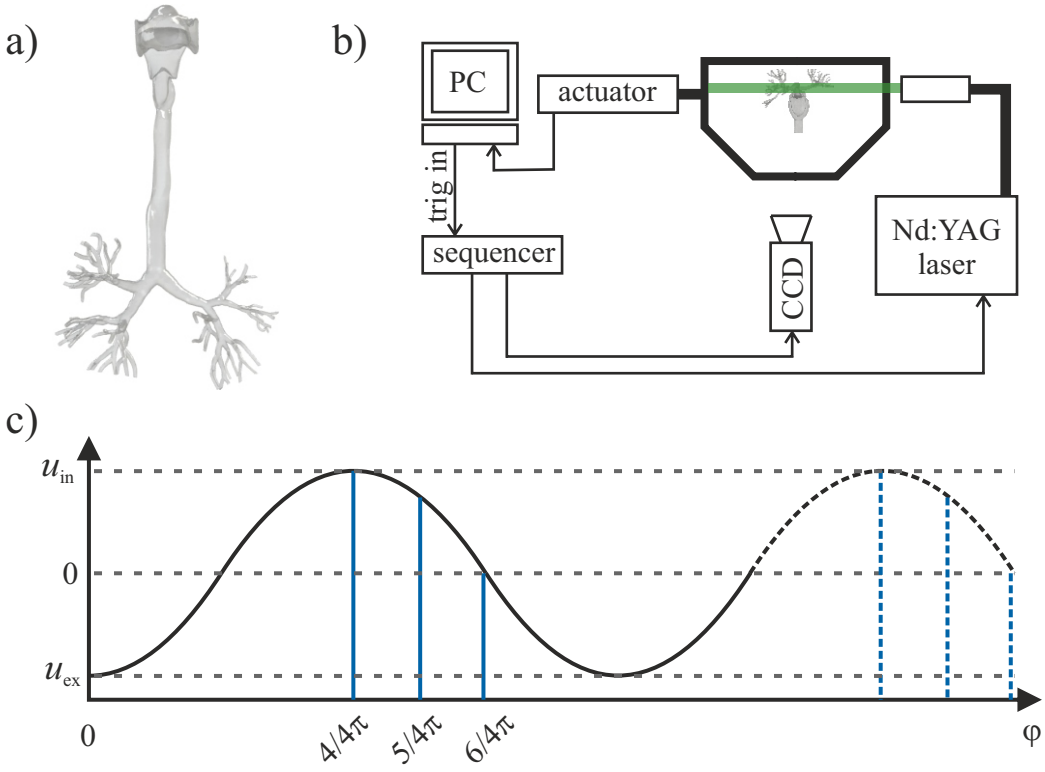

Figure 1: CAD representation of the investigated lung geometry a), schematic of the laser-optical measurement set up b), and sinusoidal signal of the driving piston velocity with indicated phase-locked measurement positions c).

reference measurements of the benchmark case (Janke et al. (2019)). The model includes the upper airways from the mouth cavity down to the fifth airway generation of the human lung and is scaled 1:1. The mean hydraulic diameter of the model's trachea is $d_T = 16.3$ mm.

In order to take advantage of refractive-index matched techniques, a water-glycerol mixture ($\nu = 8.4{\cdot}10^{-6}$ m^2/s, $\rho = 1150$ kg/m^3) is used as a working fluid. The oscillating main flow is provided by a linear actuator (G400 series, MOOG) and a piston-diaphragm pump with adjustable stroke and frequency to match different breathing parameters. Neutrally-buoyant particles are used to seed the flow ($d_p = 50\,\mu$m, $\rho = 1060$ kg/m^3, Vestosint 1174, Evonik Degussa). Illumination of the flow is provided by a double-pulsed Nd:YAG laser ($\lambda = 532$ nm, MinilitePIV, Continuum) equipped with a light-sheet optic. The particle images are recorded by a double-frame CCD camera (pco.1600, PCO). Both the laser and the camera are synchronized with the piston's movement. This allows to acquire phase-locked recordings in dependence of the piston's phase position.

The main flow is modeled with a breathing frequency of $f = 0.15$ Hz and a tidal volume of $V_T = 500$ ml, which corresponds to breathing at rest conditions in air. With the definition of the Reynolds Re and Womersley α number

$$Re = \frac{4V_T f}{\nu d_T} \qquad \alpha = \frac{d_T}{2}\sqrt{\frac{2\pi f}{\nu}} \tag{1}$$

the flow can be characterized with $Re \approx 2000$ and $\alpha = 1.9$. These numbers indicate a transitional flow state based on the Reynolds number and a rather low influence of the oscillation frequency on the mean flow profiles.

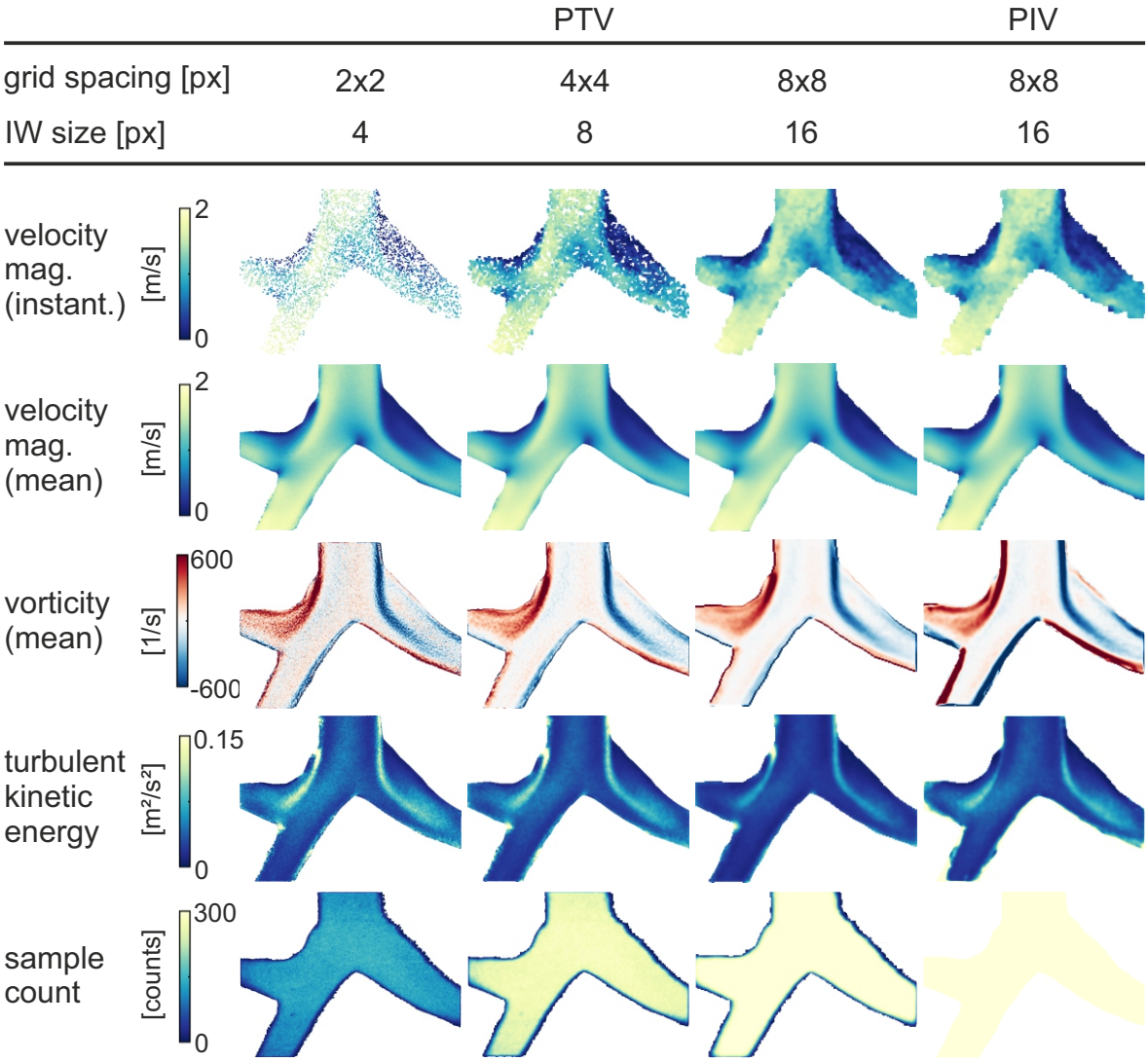

Figure 2: Comparison of different PTV interpolation grid sizes with the PIV evaluation. Shown are an exemplary instantaneaous velocity field, the mean velocity field, the vorticity field, the turbulent kinetic energy field and the number of samples used at each grid point used for the calculation of the mean values.

3 Evaluation

3.1 Image acquisition & Pre-processing

In order to test different flow conditions, double-pair images are recorded at three different phase positions during the breathing cycle. These measurement points are at peak inspiration ($\varphi = 4/4\pi$), at the decelerating inspirational phase ($\varphi = 5/4\pi$) and at the point of flow reversal from inspiration to expiration ($\varphi = 6/4\pi$, see Fig. 1). A total number of 300 image pairs are acquired for each of the phase positions, which enables the derivation of mean velocity and turbulent kinetic energy fields.

The images are recorded in several runs, due the camera's limited memory. Between the runs, the field of view of the camera shifted up to 40 px. The images are corrected and shifted before the processing, using a cross-correlation registration algorithm (Guizar-Sicairos et al. (2008)). After the correction step, the background of each image is removed by subtracting the average intensity of all images. At last, a manually drawn image mask is applied. The particle seeding density is at a moderate value of about $ppp = 0.005$. This is at the lower end for PIV applications but recommended for most PTV evaluations. The performance of the PTV algorithm for different particle densities shall be a subject of future work.

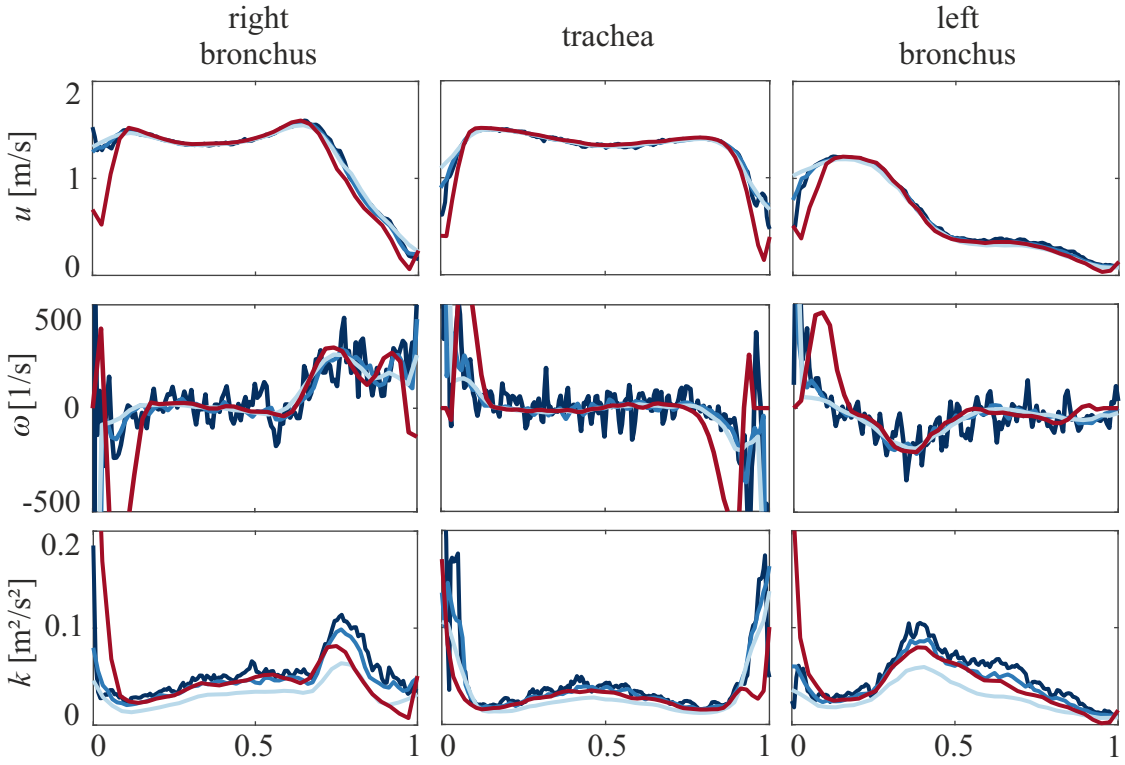

Figure 3: Velocity, vorticity and turbulent kinetic energy profiles during peak inspiration at different locations within the lung model. PIV: —, PTV 4px: —, 8px: —, 16px: —

3.2 Particle Tracking Velocimetry

As previously mentioned, the developed PTV algorithm is mainly based on the methods proposed by Fuchs et al. (2017) and developed using MATLAB R2018b (Mathworks Inc.). Within this approach, a detected particle is matched to its corresponding position in the next time frame by utilizing a statistical predictor. This predictor is build by creating a histogram of all possible displacements within a maximum field of search of the investigated particle as well as of all particles in a user defined neighborhood. The displacement with the highest bin count of the resulting histogram is expected to be the most probable particle shift. An additional three-point Gauss fit is used to further refine the prediction. If a particle is located within a tolerance distance to the estimated position, it is assigned as a correct match.
In the original work of Fuchs et al. (2017), the work has been presented as a non-iterative algorithm with the advantage of a fast flow reconstruction. While most of the particles are matched correctly after just a single pass, we found an improvement of the reconstruction by integrating a two-level iterative loop. Within the first level, velocity outliers are detected and rejected after the reconstruction by an universal outlier detection (Westerweel and Scarano (2005)) and the residual non-linked particles undergo an additional matching. Typically, three to five iterations are enough to maximize the number of reconstructed velocity vectors. The second iteration loop increases the field of search by a predefined number of increments. Especially for flows with a large range of occurring velocity magnitudes, this approach can lead to better results.
The employed particle detection method has been proposed by Crocker and Grier (1996) and has been made available by Blair and Dufresne (2005) and yields particle centroid positions with sub-pixel accuracy.
After the particle matching procedure is performed, the algorithm returns a scattered vector field for each double-frame image pair. For the comparison with the PIV data, each of these fields is interpolated onto a structured grid via a Gaussian-weighted bin averaging.
The parameters of the current evaluation are set to 25 particles as the neighborhood size for both the matching and the outlier detection. A initial field of search of 8.3 px is used, which is increased in two steps until a maximum value of 25 px. The scattered velocity fields are then interpolated on a structured grid with three different spatial resolutions. These are grids with a spacing of 2,4 and 8 px. The interpolation regions are circles with a diameter of 4, 8 and 16 px, respectively.

3.3 Particle Image Velocimetry

The PIV evaluation of the recorded images is performed within the commercially available software DaVis 9 (LaVision GmbH). The pre-processed images are imported into the software. The used PIV algorithm is a cross-correlation (FFT) multi-pass approach with decreasing window width, starting from an interrogation window size of 32 px and ending at a size of 16 px, each with an overlap of 50 %. While the first window size uses just a single pass, the second IW's pass count is increased to three. The post-processing of the yielded vector fields is performed by an universal outlier detection, an interpolation of empty vector spaces and finally a denoising step. As the PIV algorithm proofed to produce comparably good results according to the latest International PIV Challenge Kähler et al. (2016), we expect the software to be a reliable reference.

4 Results

A first comparison between the PIV and the PTV evaluation is shown in Fig. 2, which shows the overall flow field during peak inspiration inside the main carina for all different grid sizes. Besides the velocity magnitude (instantaneous and averaged), the mean vorticity, the turbulent kinetic energy and the sample count are displayed. The sample count represents the number of velocity vectors, which have been used for the derivation of the mean values. As it can be seen in the instantaneous fields for a grid spacing of 2 and 4 px, the seeding density is too low to get flow information for every grid point. Since no further interpolation on these missing spots are performed, the sample count decreases in these regions in contrast to the PIV evaluation. For the PTV results at a grid resolution of 8 px and a window size of 16 px the sample count corresponds to the number of acquired images. Just near the wall, the sample count decreases significantly. This is probably due to a low amount of tracer particles in these areas and a consequence of the background removal process. To conclude this paragraph, a higher spatial resolution can be achieved with PTV but at the cost of a decreasing number of effective samples. In order to achieve a comparably high sample count for a grid spacing of 2 px as in PIV with 8 px (four times better spatial resolution), one would have to record approximately three times the images as it would be necessary for PIV. This may be impracticable for some experiments but shows, that the PTV method can produce mean velocity fields with an increasing spatial resolution by raising the number of acquired images. Such an effect is hardly achievable with common PIV algorithms.
Despite the low sample count for the higher resolved grids, the mean velocity fields show no qualitative differences according to Fig. 2. But the derived values, such as the vorticity and the turbulent kinetic energy, present noisier fields.

For a better quantitative comparison, profile lines across the trachea, the right and left main bronchus are plotted in Fig. 3. Included in this figure are the mean velocity u, the vorticity ω and the turbulent kinetic energy k. As already indicated in the previous paragraph, all mean velocity profile lines overlap for the most parts. Larger differences occur in near wall regions. The effect of the non-converged finer grids is clearly visible for the vorticity. Especially the results for a grid size of 2 px show strong fluctuations along the profile, but the mean trend corresponds well with the other grid resolutions. A coarse spatial filtering can lead to an underestimation of the turbulent kinetic energies (Saarenrinne et al. (2001)). Looking at the corresponding profiles, a clear trend towards higher k values for a finer grid is observable. For the same window size and the same grid spacing, the turbulent kinetic energies calculated from the PIV results are slightly lower than from the PTV results.
The last point of the study is to test the ability of both evaluation methods of how they handle different mean particle displacements. For peak inspiration ($\varphi = 4/4\pi$) the mean particle shift is approximately 6 px, for the phase position $\varphi = 5/4\pi$ it is around 4 px and at the point of flow reversal ($\varphi = 6/4\pi$), the particle displacement is in average just 0.3 px. The same profile plots as already introduced before are shown in Fig. 4 again but now in dependence of the three phase positions and just for the line across the right main bronchus. As the results for a corresponding grid spacing between PTV and PIV have shown to be the most identical, the comparison is limited to this parameter set. In accordance to the previous results, the profile lines indicate the same characteristics as described above (overall good agreement, larger deviations in wall-near regions, higher k values for PTV) for the cases of peak and decelerating inspiration. When comparing the results for flow reversal, the relative deviations are larger. During the PTV processing it is necessary to compute two sub-pixel particle positions in order to calculate the displacement. In contrast, the PIV algorithm just has to find a single peak within the correlation function. This aspect might lead to a higher uncertainty of the PTV results for small particle movements and explain the occurring differences between both evaluation approaches.

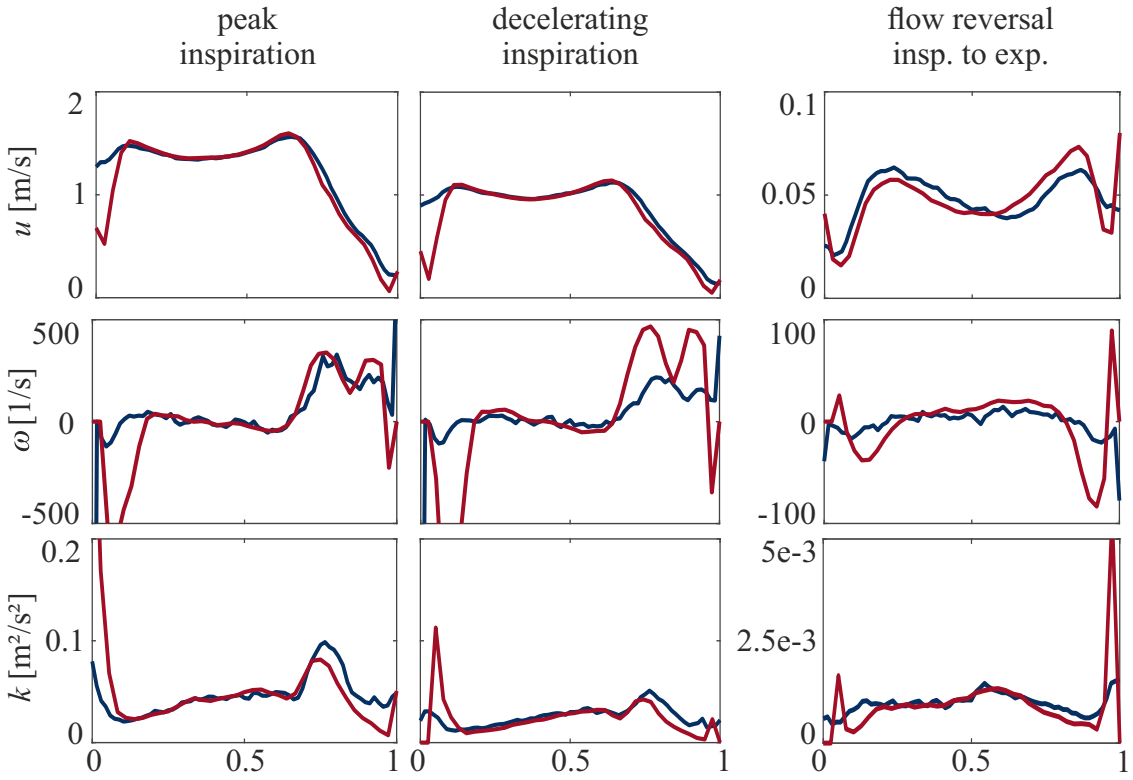

Figure 4: Velocity, vorticity and turbulent kinetic energy profiles within the right bronchus during different phase positions. PIV: —, PTV: 8px —

5 Conclusion

The oscillatory flow within a realistic lung geometry was measured by means of PIV and PTV for three different phase positions during the breathing cycle (Re = 2000, α = 1.9). The aim of this experiment was the comparison of an in-house developed 2D-PTV algorithm with an established PIV software. Both evaluation approaches led to equal velocity fields for most areas. Larger deviations occur at near-wall positions and indicate differences in how both methods can resolve these velocity vectors. While the velocity profiles seem smooth for even small PTV interpolation windows, derived measures, such as the vorticity, show the contrary. A dependence of the turbulent kinetic energies from the chosen grid resolution could be confirmed, as this effect has already been reported in previous studies.
Besides the influence of the spatial resolution, the effect of different mean particle displacement has been investigated. For peak inspiration and the decelerating phase, comparable velocity profiles were present. At the point of flow reversal, with mean particle shift less than a pixel, the results from the PTV and PIV evaluation differ stronger.
All in all, the successful implementation of the PTV method could be shown. Already known effects from the literature, such as different near-wall resolution capabilities, a different handling of very small displacements and slight deviations in the estimation of the turbulent kinetic energies could be reproduced.

Acknowledgements

The financial support of this study by the Deutsche Forschungsgemeinschaft (DFG grant No. BA 4995/2-1) is gratefully acknowledged.

References

Adler K and Brücker C (2007) Dynamic flow in a realistic model of the upper human lung airways. *Experiments in Fluids* 43:411–423

Blair D and Dufresne E (2005) The Matlab Particle Tracking Code Repository https://site.physics.georgetown.edu/matlab/. *accessed 13 02 2019*

Crocker J and Grier D (1996) Methods of Digital Video Microscopy for Colloidal Studies. *Journal of Colloid and Interface Science* 179:298–310

Fresconi FE and Prasad AK (2007) Secondary Velocity Fields in the Conducting Airways of the Human Lung. *Journal of Biomechanical Engineering-Transactions of the ASME* 129:722–732

Fuchs T, Hain R, and Kähler CJ (2017) Non-iterative double-frame 2D/3D particle tracking velocimetry. *Experiments in Fluids* 58:1–5

Große S, Schröder W, Klaas M, and Klöckner A (2007) Time resolved analysis of steady and oscillating flow in the upper human airways. *Experiments in Fluids* 42:955–970

Guizar-Sicairos M, Thurman ST, and Fienup JR (2008) Efficient subpixel image registration algorithms.. *Optics letters* 33:156–8

Janke T, Koullapis P, Kassinos S, and Bauer K (2019) PIV measurements of the SimInhale benchmark case. *European Journal of Pharmaceutical Sciences* 133:183–189

Kähler CJ, Astarita T, Vlachos PP, and Sakakibara J (2016) Main results of the 4th International PIV Challenge. *Experiments in Fluids* 57:1–71

Kähler CJ, Scharnowski S, and Cierpka C (2012) On the resolution limit of digital particle image velocimetry. *Experiments in Fluids* 52:1629–1639

Koullapis P, Kassinos SC, Muela J, Perez-Segarra C, Rigola J, Lehmkuhl O, Cui Y, Sommerfeld M, Elcner J, Jicha M, Saveljic I, Filipovic N, Lizal F, and Nicolaou L (2018) Regional aerosol deposition in the human airways: The SimInhale benchmark case and a critical assessment of in silico methods. *European Journal of Pharmaceutical Sciences* 113:77–94

Lizal F, Elcner J, Hopke PK, Jedelsky J, and Jicha M (2012) Development of a realistic human airway model. *Proceedings of the Institution of Mechanical Engineers, Part H: Journal of Engineering in Medicine* 226:197–207

Saarenrinne P, Piirto M, and Eloranta H (2001) Experiences of turbulence measurement with PIV. *Measurement Science and Technology* 12:1904–1910

Westerweel J and Scarano F (2005) Universal outlier detection for PIV data. *Experiments in Fluids* 39:1096–1100